Inorganic Chemistry

Article

pubs.acs.org/IC

Trimetallic Borohydride $Li_3MZn_5(BH_4)_{15}$ (M = Mg, Mn) Containing Two Weakly Interconnected Frameworks

Radovan Černý,*[,†] Pascal Schouwink,[†] Yolanda Sadikin,[†] Katarina Stare,[†,‡] L'ubomír Smrčok,[§] Bo Richter,[∥] and Torben R. Jensen[∥]

[†]Laboratory of Crystallography, University of Geneva, 24-quai Ernest-Ansermet, CH-1211 Geneva, Switzerland

[‡]Faculty of Chemistry and Chemical Technology, University of Ljubljana, Aškerjeva 5, SI-1000 Ljubljana, Slovenia

[§]Institute of Inorganic Chemistry, Slovak Academy of Sciences, Dúbravská cesta 9, SK-845 36 Bratislava, Slovak Republic

[∥]Center for Materials Crystallography (CMC), Interdisciplinary Nanoscience Center (iNANO), and Department of Chemistry, Aarhus University, Langelandsgade 140, DK-8000 Århus C, Denmark

Supporting Information

ABSTRACT: The compounds, $Li_3MZn_5(BH_4)_{15}$, M = Mg and Mn, represent the first trimetallic borohydrides and are also new cationic solid solutions. These materials were prepared by mechanochemical synthesis from $LiBH_4$, MCl_2 or $M(BH_4)_2$, and $ZnCl_2$. The compounds are isostructural, and their crystal structure was characterized by in situ synchrotron radiation powder X-ray and neutron diffraction and DFT calculations. While diffraction provides an average view of the structure as hexagonal (a = 15.371(3), c = 8.586(2) Å, space group $P6_3/mcm$ for Mg-compound at room temperature), the DFT optimization of locally ordered models suggests a related ortho-hexagonal cell. Ordered models that maximize Mg−Mg separation have the lowest DFT energy, suggesting that the hexagonal structure seen by diffraction is a superposition of three such orthorhombic structures in three orientations along the hexagonal c-axis. No conclusion about the coherent length of the orthorhombic structure can be however done. The framework in $Li_3MZn_5(BH_4)_{15}$ is of a new type. It contains channels built from face-sharing $(BH_4)_6$ octahedra. While X-ray and neutron powder diffraction preferentially localize lithium in the center of the octahedra, thus resulting in two weakly interconnected frameworks of a new type, the DFT calculations clearly favor lithium inside the shared triangular faces, leading to two interpenetrated **mco**-nets (**mco**-c type) with the basic tile being built from three **tfa** tiles, which is the framework type of the related bimetallic $LiZn_2(BH_4)_5$. The new borohydrides $Li_3MZn_5(BH_4)_{15}$ are potentially interesting as solid-state electrolytes, if the lithium mobility within the octahedral channels is improved by disordering the site via heterovalent substitution. From a hydrogen storage point of view, their application seems to be limited as the compounds decompose to three known metal borohydrides.

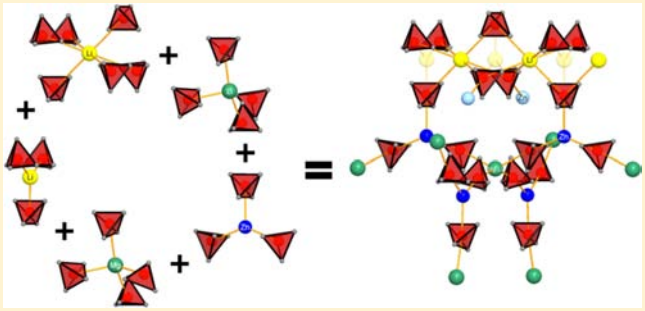

INTRODUCTION

Bimetallic borohydrides (also called tetrahydroborates) currently attract considerable attention due to their fascinating structural diversity, adjustable hydrogen storage properties, and Li-ion conductivity for future mobile applications.[1,2] A variety of new members of this group of compounds have been discovered during the past few years.[3] Several series of bimetallic borohydrides have been structurally characterized: $MSc(BH_4)_4$ (M = Li, Na, K),[4−6] $KY(BH_4)_4$,[7] $MZn_2(BH_4)_5$ (M = Li, Na) and $NaZn(BH_4)_3$,[8,9] $Li_4Al_3(BH_4)_{13}$[10] as well as $NaAl(BH_4)_4$,[11] and $KM(BH_4)_3$ (M = Mn, Cd, Zn), $K_2M(BH_4)_4$ (M = Mg, Mn, Cd, Zn), and $K_3Mg(BH_4)_5$.[12−14] These compounds are described as salts containing homoleptic complex anions such as tetrahedral $[Sc(BH_4)_4]^-$, $[Al(BH_4)_4]^-$, and $[Zn(BH_4)_4]^{2-}$ or triangular $[Zn(BH_4)_3]^-$ charge-balanced by alkali metal counter-cations. Borohydrides with $[Al(BH_4)_4]^-$ anion contain a significant amount of chloride replacing for borohydride when prepared from $AlCl_3$. The $MZn_2(BH_4)_5$ (M = Li, Na) compounds may be rationalized as built from two interpenetrated frameworks containing a binuclear complex anion $[Zn_2(BH_4)_5]^-$. In addition to bimetallic borohydrides with ordered structures, cationic solid solution borohydride $Mg_xMn_{(1-x)}(BH_4)_2$ was recently characterized.[15] No borohydride containing more than two different metallic cations has been reported to date.

In our search for new bimetallic borohydrides in the systems M−Zn−BH_4 (M = Mg, Mn), we have studied ball-milled mixtures of $MgCl_2$ and $MnCl_2$, with $ZnCl_2$ and $LiBH_4$. Alkali metal borohydrides are used in such metathesis reactions as a source of borohydride, and usually form alkali metal halides as reaction product. The theoretically studied[16] Mg−Zn borohy-

Received: May 8, 2013
Published: August 22, 2013

   dx.doi.org/10.1021/ic401139k | Inorg. Chem. 2013, 52, 9941−9947

dride did not form, but surprisingly a new trimetallic borohydride $Li_3MZn_5(BH_4)_{15}$ was formed in our ball-milled mixtures. Later, the compound was prepared by using $M(BH_4)_2$ instead of MCl_2, resulting in a homoleptic complex. The reaction of $Mg(BH_4)_2$ with $ZnCl_2$ in diethyl ether or diglyme solutions was studied in ref 17. A mixed compound $MgZn(BH_4)_4$ was reported, but without the crystal structure.

Here, we report on the synthesis, crystal structure, and ionic conductivity of the first trimetallic borohydrides $Li_3MZn_5(BH_4)_{15}$ (M = Mg, Mn).

EXPERIMENTAL SECTION

Synthesis, Mg-Based Samples. Mixtures of $LiBH_4$ (>95%, Aldrich), anhydrous $MgCl_2$ (>98%, Aldrich), and anhydrous $ZnCl_2$ (>99.99%, Aldrich) with molar ratios 8:2:2, 8:1:3, 8:3:1, and 6:1:2 were manually premixed using an agate mortar, and then mechanically milled.[18] The milling process was carried out in a Fritsch Pulverisette 7 high-energy planetary ball-milling system. A 25 mL stainless steel grinding bowl sealed with a lid having a Viton O-ring and three stainless steel balls of 15, 12, and 10 mm in diameter were used as milling medium. The rotational speed of milling was set to 600 rpm. The ball mass to powder mass ratio was fixed to 25:1. The milling was stopped for 5 min (cooling brake) every 10 min to avoid heating of the system as well as agglomeration of the powder on the walls of the grinding bowl; the previous two-step process was repeated 35 times. All samples were handled under inert conditions (argon). The samples synthesized with $MgCl_2$ will be labeled a-Mg.

Motivated by the first structural results from $MgCl_2$-containing samples, a mixture of $LiBH_4$ (>95%, Aldrich), $Mg(BH_4)_2$ (>99%, prepared according to ref 19), and anhydrous $ZnCl_2$ (>99.995%, Aldrich) in the molar ratio 10:2:4 was prepared using the above given milling parameters. The aim was to decrease the amount of chlorine in the sample, and this sample will be labeled b-Mg.

Sample labeled c-Mg was prepared for neutron powder diffraction experiment. In total, 2.5 g of powder was prepared in five separate millings from $Li^{11}BD_4$, $Mg(^{11}BD_4)_2$ (see the Supporting Information for the preparation), and anhydrous $ZnCl_2$ (>99.995%, Aldrich) in the molar ratio 10:2:4 using the above given milling parameters.

Synthesis, Mn-Based Samples. A manganese-based sample was first synthesized in the molar ratio 6:1:2 using anhydrous $MnCl_2$ (>99.999%, Aldrich). The two-step ball-milling process (2 min milling + 2 min cooling brake) was repeated 90 times. This sample will be labeled a-Mn. Low-chlorine manganese-based sample was synthesized from a mixture of $LiBH_4$ (>95%, Aldrich), $Mn(BH_4)_2$ (>99%, prepared by a procedure similar to that of $Mg(BH_4)_2$ according to ref 13), and anhydrous $ZnCl_2$ (>99.995%, Aldrich) in the molar ratios 13:2:5, 13:1:5, and 15:2:3 using the same two-step ball-milling process but repeated 60 times. The samples will be labeled b-Mn. The list of prepared samples is given in the Supporting Information as Table S1.

In Situ Synchrotron Radiation Powder X-ray Diffraction (SR-PXD). One set of in situ time-resolved synchrotron radiation powder X-ray diffraction data (SR-PXD) was collected on the samples a,b-Mg,Mn at the Swiss-Norwegian Beamlines (SNBL) at the European Synchrotron Radiation Facility (ESRF) in Grenoble, France. A glass capillary (o.d. 0.5, 0.8, or 1 mm) with the sample was heated from 150 to 500 K at a rate of 1, 1.5, or 2 K/min, while SR-PXD data were collected (T-ramp). The temperature was controlled with the Oxford Cryostream 700+ or with a heat-blower. The data were collected using a MAR345 image plate detector at a sample to detector distance of 250 mm, and the radiation with the wavelength of λ = 0.69671(1), 0.69776(1), 0.70138(2), or 0.75274(1) Å calibrated by an external silicon standard. The capillary was oscillated by 60° during exposure to the X-ray beam for 30−60 s, followed by a readout for 83 s. All obtained raw images were transformed to 2D-powder patterns using the FIT2D[20] program. A high-resolution SR-PXD data set was collected at room temperature on the sample a-Mg prepared with the ratio 6:1:2 using the high-resolution powder diffractometer at the SNBL equipped with a multicrystal analyzer, and the wavelength of λ = 0.50120(1) Å.

Another set of in situ SR-PXD data was collected on the samples a-Mg at the Materials Science Beamline at the Swiss Light Source (SLS) in PSI Villigen, Switzerland. A glass capillary (o.d. 0.8 or 1 mm) with the sample was heated from 293 to 623 K at a rate of 1, 4, or 8 K/min, and the powder diffraction data were collected at temperature steps of 1, 4, and 8 K, respectively. Temperature was controlled with the STOE high temperature attachment. The data were collected using a MYTHEN-II silicon strip detector with the radiation wavelength of λ = 0.72960(1) Å calibrated by an external silicon standard. The capillary was spun during the exposure to the X-ray beam.

Selected T-ramps (i.e., powder diffraction patterns as a function of temperature) are shown as Figures S1−S3.

Powder Neutron Diffraction (PND). Powder diffraction patterns of sample c-Mg were measured at room temperature and at 15 K using the HPRT diffractometer (PSI, Villigen). The high intensity mode and a wavelength of 1.8857 Å were used. The temperature was controlled by a Displex closed cycle refrigerator.

Crystal Structure Solution and Refinement. The crystal structure of $Li_3MgZn_5(BH_4)_{15}$ was first solved using the room temperature SLS data of sample a-Mg 8:2:2. Nineteen powder diffraction peaks that vanish at the same time at 393 K in the T-ramp were indexed with DICVOL04[21] in a hexagonal lattice with a = 15.374(1), c = 8.5688(6) Å, V = 1754.1(3) Å^3 at room temperature (values from the final Rietveld refinement, sample a-Mg 8:2:2; see Figure S6). Systematic extinctions clearly pointed toward extinction symbol *P-c-* leaving the choice between three hexagonal and two trigonal space groups. The structure was modeled with 2 Zn, 1 Mg, 1 Li atom, and 3 semirigid ideal tetrahedra BH_4 with one common refined B−H distance, and was finally solved in the space group $P6_3/mcm$ (i.e., highest symmetry compatible with the extinction symbol) with the direct space method program FOX[22] using appropriate antibump distances between all atoms. Impurity phases (see Table S1) were included with their fixed structural models. The resulting structure composed from the same number of independent building blocks as used for modeling in FOX was then refined by the Rietveld method using the TOPAS program.[23] The RT data of the sample b-Mg 10:2:4 were used for the final Rietveld refinement because of a lower number of impurity phases. Refined atomic coordinates are given in Table S2, and the Rietveld plot is in Figure S7. The site (6*g*) was found during the refinement to be occupied by both Mg and Li. The occupancy of the Li site (2*b*) was constrained to the occupancy of the 6*g* site to keep the balanced charge as $3x - 1$ where x is the Li fraction on the site 6*g*. The refinement of neutron data at 15 K confirmed the room temperature structural model, but suffered from lower angular resolution induced by synthesis of several batches of the powder needed for bigger volume of the neutron diffraction specimen. Moreover, the refinement of the mixed Li/Mg site was unstable when using the neutron data due to low scattering power of the Li−Mg mixture in the ratio 2:1 (b_c = 1.575 fm) as compared to ^{11}B (b_c = 6.65 fm) and D (b_c = 6.671 fm), and the atomic coordinates were finally fixed to the X-ray results. The refined atomic coordinates are given in Table S3. Refinement of the manganese-based compound was performed using X-ray powder diffraction data measured at room temperature on sample b-Mn 13:2:5 and the structural model of the magnesium-based compound. Refined atomic coordinates are given in Table S4. Rietveld plots are given as Figures S6−S10, and phase composition of the samples and agreement factors of Rietveld refinement are in Table S1. Corresponding CIF files are given in the Supporting Information. The symmetry of refined structures including hydrogen atoms has been checked with the routine ADDSYM in the program PLATON,[24] and the space group $P6_3/mcm$ was confirmed.

DFT Calculation Details. All of the solid-state calculations were performed using the VASP code.[25,26] To optimize the structures, two pseudopotentials developed for solid-state calculations, PBESOL[27] and AM05,[28] were used. Positions of all of the atoms in the cell were fully relaxed, either keeping the lattice parameters fixed at the experimental values or relaxing them along with the atomic coordinates. When optimizing the lattice parameters, empirical dispersion correction by

dx.doi.org/10.1021/ic401139k | Inorg. Chem. 2013, 52, 9941−9947

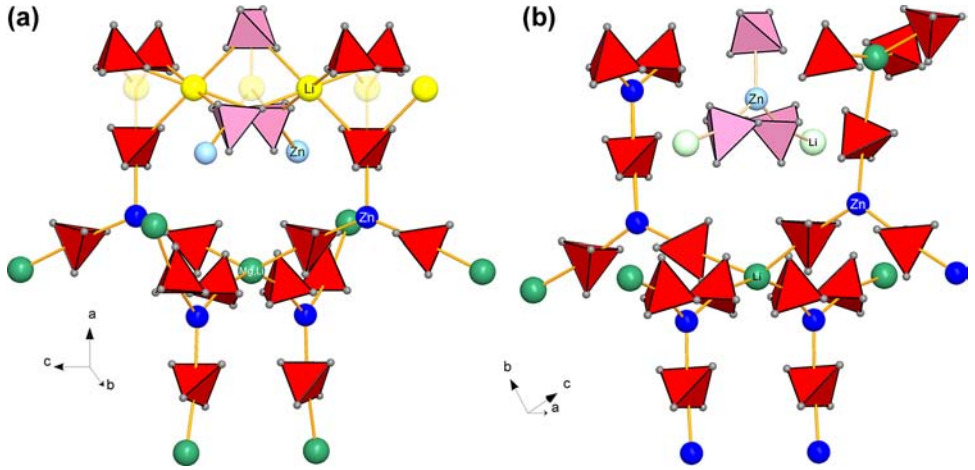

Figure 1. Part of one structural framework in hexagonal $Li_3MgZn_5(BH_4)_{15}$ (a, left) and in orthorhombic $LiZn_2(BH_4)_5$ (b, right). The Zn atoms are in blue, mixed Li/Mg site (a, left) and Li site (b, right) are in green, and BH_4 tetrahedra are in red. A small part of the second framework in both compounds is shown in light colors. Lithium in octahedral and triangular coordination in the face-sharing octahedral chain running along the *c*-axis in $Li_3MgZn_5(BH_4)_{15}$ is shown as full and transparent yellow atoms, respectively.

ref 29 or that by ref 30 as implemented in VASP code[31] was applied. Plane waves formed a basis set, and the calculations were performed using the projector-augmented wave method[32,33] and atomic pseudopotentials.[34] The energy cutoff controlling the accuracy of structure optimization calculations was set to 700 eV, and convergence criterion was set to 10^{-7}. Considering the size of the computational cell (336 atoms), the Brillouin zone was sampled just in Γ point.

Ionic and Electronic Conductivity. Ionic and electronic conductivities were measured at room temperature with electrochemical impedance spectroscopy (EIS) and chronoamperometry (CA), respectively. The EIS measurement was performed using a Hewlett-Packard 4192A LF impedance analyzer (frequency range from 10 Hz to 13 MHz, applied voltage 1 V) and a Novocontrol sample cell BDS 1200. The powder was pressed at 200 MPa and room temperature without sintering into a pellet (diameter 10 mm, thickness ~0.8 mm, corresponding to 75% of the density calculated from the crystal structure at ambient conditions),which was then sandwiched between lithium foil electrodes stuck onto a gold sample holder in the airtight sample cell BDS 1308. Sample loading was carried out under Ar atmosphere.

Nyquist plots of the complex impedance (imaginary part Z_{im} as a function of the real part Z_{re}) provide the resistances of the sample obtained from the diameter of the first semicircle. The total ionic conductivity is calculated from the ionic resistance and measured specimen thickness and its cross-sectional area. The Nyquist plot is shown in Figure S4.

CA measurements were performed with ion-blocking gold electrodes in a chronoamperometric mode. The voltage was increased from 0.1 to 0.5 V with a step size of 0.1 V and a step time of around 10 min. The resulting current was measured using a PC-controlled NI-USB6259 National Instrument multimeter. The measured data are shown in Figure S5, for each constant voltage applied, and the current eventually drops to a constant value. The electronic conductivity was then determined using Ohm's law.

RESULTS AND DISCUSSION

Synthesis and Initial Phase Analysis. According to the observed compounds in the powder diffraction patterns and according to numerous Rietveld refinements, the ideal composition for the synthesis of $Li_3MZn_5(BH_4)_{15}$ using MCl_2 (samples a-Mg and a-Mn) can be formulated as

$$15LiBH_4 + 5MCl_2 + 5ZnCl_2 \rightarrow Li_3MZn_5(BH_4)_{15} + 4LiCl + 4Li_2MCl_4 \quad (1)$$

because Li_2MCl_4 was the only reaction byproduct observed in all syntheses (except for the chlorine-deficient sample a-Mg mixture 8:3:1). However, the formation of $LiZn_2(BH_4)_5$ was often observed due to a competing side-reaction, which shifts the ideal reaction ratio away from 15:5:5.

The reaction scheme for formation of $Li_3MZn_5(BH_4)_{15}$ using $M(BH_4)_2$ (samples b,c-Mg and b-Mn) is

$$13LiBH_4 + M(BH_4)_2 + 5ZnCl_2 \rightarrow Li_3MZn_5(BH_4)_{15} + 10LiCl \quad (2)$$

Formation of $LiZn_2(BH_4)_5$ was also observed in this case, due to which the ideal reaction ratio maximizing the yield of $Li_3MZn_5(BH_4)_{15}$ was thus found to be approximately 10:2:4, instead of the assumed 13:1:5. The 15 produced samples of $Li_3MZn_5(BH_4)_{15}$ were mixtures of 3−6 different compounds confirmed by Rietveld refinement, which also provide the sample compositions; see Table S1.

Thus, the formation of $Li_3MZn_5(BH_4)_{15}$ was observed in all ball-milled mixtures alluding to the high stability of these two new trimetallic borohydrides formed that contain three different cations in the structure.

Decomposition Analysis by in Situ Time-Resolved SR-PXD. $Li_3MgZn_5(BH_4)_{15}$ decomposes at 393 K to three known borohydrides as it is observed from the T-ramp of the sample a-Mg 8:2:2 (Figure S1):

$$2Li_3MgZn_5(BH_4)_{15} \rightarrow 5LiZn_2(BH_4)_5 + LiBH_4 + 2Mg(BH_4)_2 \quad (3)$$

The decomposition is then immediately followed by the reaction:

$$Mg(BH_4)_2 + 4LiCl \rightarrow 2LiBH_4 + Li_2MgCl_4 \quad (4)$$

which is also observed for ball-milled mixtures of $LiBH_4$:$MgCl_2$:$MnCl_2$.[15]

At 397 K, $LiZn_2(BH_4)_5$ decomposes according to the previously published reaction:[8]

$$LiZn_2(BH_4)_5 \rightarrow 2Zn + LiBH_4 + 2B_2H_6 + 2H_2 \quad (5)$$

dx.doi.org/10.1021/ic401139k | Inorg. Chem. 2013, 52, 9941−9947

The samples prepared using $M(BH_4)_2$ instead of MCl_2 show the same thermal decomposition route (Figures S2 and S3) as sample a-Mg 8:2:2, the only difference being the onset of decomposition of $Li_3MgZn_5(BH_4)_{15}$, which occurs already at 368 K in the pure compound, probably due to eutectic behavior of $Li_3MgZn_5(BH_4)_{15}$ and residual $Mg(BH_4)_2$ in the ball-milled mixture b-Mg 10:2:4. On the other hand, the decomposition of $Li_3MnZn_5(BH_4)_{15}$ in b-Mn 15:2:3 containing residual $Mn(BH_4)_2$ occurs at 385 K.

The cell volume and lattice parameters of $Li_3MgZn_5(BH_4)_{15}$ as a function of temperature (Figure S13) were determined by sequential Rietveld refinement using the SR-PXD data collected on sample a-Mg 6:1:2. The temperature dependence can be approximated by a linear function within the interval 200−325 K, and it starts to deviate from the linearity close to low and high temperature limits. The deviation is not due to changes in the chemical composition of the compound (Cl substitution on the borohydride sites or a change of Li/Mg ratio) as it follows from Rietveld refinement. No deviation from the hexagonal metric was detected in the low-resolution data from synchrotron (down to 150 K), neutron (15 K) powder diffraction, neither from the high resolution SR-PXD measured at room temperature on the magnesium-based sample.

Crystal Structure. $Li_3MZn_5(BH_4)_{15}$, M = Mg or Mn, crystallizes with identical structures (space group $P6_3/mcm$); see Figure 1a. The neutron data collected on $Li_3MgZn_5(^{11}BD_4)_{15}$ have confirmed the structural results of the X-ray data, but their lower angular resolution did not allow one to exploit fully the advantage of the strong scattering from deuterium. We will focus therefore in the following on the X-ray results of the Mg analogue only. $Li_3MgZn_5(BH_4)_{15}$ contains two Zn sites with planar triangular coordination by three BH_4 groups. One zinc atom, Zn1, is located on Wyckoff site 4*c* with site symmetry $\bar{6}$, and it is coordinated by an equilateral triangle formed by three equivalent borohydride groups centered on B3, with Zn−B distances of 2.25(1) Å. The second zinc atom, Zn2, is located on Wyckoff site 6*g* with site symmetry *m*2*m*, and with Zn−B distances of 2.24(1) and 2.34(1) Å for B2 and B1, respectively. The B−Zn−B angles are of 111.0(3)° and 138.0(3)°. The orientation of BH_4 groups was constrained during the refinement using X-ray data (but not for neutron data) to constrain the trigonal prismatic coordination of Zn by six H atoms as retrieved from neutron powder diffraction data of the related compound $LiZn_2(^{11}BD_4)_5$.[35] The Zn−H distances in $Li_3MgZn_5(BH_4)_{15}$ are within 1.84(1)−1.93(1) Å, in good agreement with ref 35.

The mixed occupied Li/Mg site (6*g*) is coordinated by four BH_4 groups of two B2 and two B3 atoms in nearly saddle-like coordination with the B−Li/Mg−B angles between 95.0(1)° and 155.8(4)°, and Li/Mg−B distances within 2.41(1)−2.48(1) Å. The tetrahedral BH_4 groups are oriented with their edges toward Li/Mg with Li/Mg−H distances of 1.89(1)−2.21(1) Å. A similar saddle-like coordination of Li was observed in the structurally related $LiZn_2(BH_4)_5$,[8,35] and for Mg it falls within the range of observed deformed tetragonal coordinations in $Mg(BH_4)_2$.[36]

The site 2*b* that is occupied only by Li has deformed octahedral coordination by six BH_4 groups of the atom B1 with Li−B distance of 2.94(1) Å (Figures 1 and 2). The B−Li−B *cis*-angles are 72.60(1)° and 107.40(1)°. The symmetry constrained orientation of the BH_4 group results in the H-vertex coordination of Li with Li−H distances of 1.82(1) Å. Such coordination of Li is observed for the first time in borohydrides,

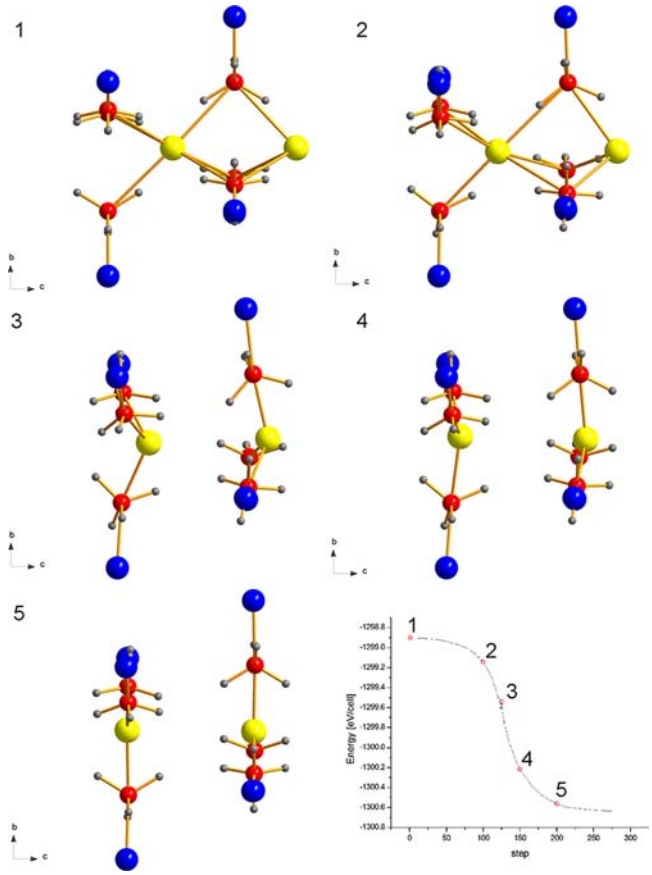

Figure 2. Chain of face-sharing $Li(BH_4)_6$ octahedra running along the *c*-axis and viewed approximately along the *a*-axis of the orthohexagonal cell of $Li_3MgZn_5(BH_4)_{15}$. Transition of Li from the octahedral coordination on the site 2*b* to the triangular coordination on the site 2*a* of the hexagonal structure (s.g. $P6_3/mcm$) as proposed by DFT optimization of the ordered orthohexagonal model no. 4. The Zn atoms are in blue, Li are in yellow, B are in red, and H are in gray. Corresponding DFT energies are shown as red circles.

but compares well to $LiSc(BH_4)_4$ where the H-vertex coordination of the disordered Li site was considered as one of the possibilities.[4] The $Li(BH_4)_6$ octahedra form face-sharing chains along the *c*-axis. The occupancy of the Li site 2*b* was refined but constrained to the Li/Mg site 6*g* to conserve charge balances as specified in the experimental part. The occupancy of the Li site 2*b* refines in all samples, Mg and Mn analogues, to 100% within the experiment accuracy. As it is shown below, the DFT optimization of the experimental structure favors the position of Li to be centered inside the shared triangular face rather than in the center of the octahedron.

The coordination of $[BH_4]^-$ anions by Li/Mg and Zn cations is nearly linear for B2 and B3 with cation−B−cation angles of 176.3(4)° and 165.5(4)°, respectively, and planar triangular for B1 with cation−B−cation angles 93.8(1)° and 133.1(1)°. The shortest H−H distances between two BH_4 groups are of 2.35(1) Å.

DFT Modeling of Ordered Structure. The chemical composition of $Li_3MZn_5(BH_4)_{15}$ as refined by Rietveld refinement using the hexagonal structural model corresponds to a stoichiometric formula in all samples, and does not vary with temperature (see Tables S2−S4). This suggests that the disordered Li/Mg site 6*g* and the hexagonal symmetry is only an average view of the crystal structure. We have verified this

dx.doi.org/10.1021/ic401139k | Inorg. Chem. 2013, 52, 9941−9947

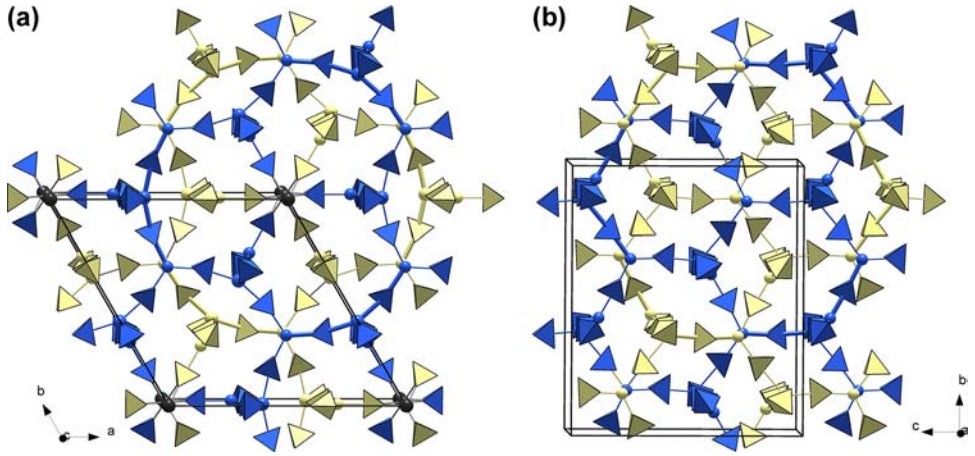

Figure 3. Structural projections of hexagonal $Li_3MgZn_5(BH_4)_{15}$ along the c_{hex}-axis (a, left), and of orthorhombic $LiZn_2(BH_4)_5$ along the a_{ortho}-axis (b, right). The two interpenetrated frameworks are shown in both drawings as yellow and blue, respectively. Structural fragment with an ideal hexagonal symmetry in $Li_3MgZn_5(BH_4)_{15}$ and pseudohexagonal symmetry in $LiZn_2(BH_4)_5$ is drawn as bold bonds.

hypothesis by a series of solid-state DFT calculations of ordered structural models. Five fully ordered models were created in an orthohexagonal lattice and are shown in Figure S11: Model 1 is described in space group *Cmcm*, derived from a maximal nonisomorphic subgroup of $P6_3/mcm$, and allowing for a fully ordered distribution of Li and Mg on the hexagonal site 6*g*. The important feature of this distribution is that it maximizes distances between Mg atoms and conserves chemical composition and the periodicity of the orthohexagonal lattice. Models 2 and 5 are two further possible distributions with maximized Mg−Mg distances, and both can exist in two variants related by the mirror plane ($x1/2z$). If we assume that the three distributions (model 1 and two variants of the model 2 or 5) can exist within the crystal with equal probabilities, then the superposition of these three distributions (check in Figure S11) results in the hexagonal symmetry $P6_3/mcm$ with the site 6*g* occupied by 2/3 of Mg and 1/3 of Li, as suggested by Rietveld refinement. If the Mg−Mg separations are not maximized, only two other distributions of Mg and Li are possible within the orthohexagonal lattice. These are models 3 and 4.

Models 1−5 were optimized by solid-state DFT calculation using different approximations (Table S5). The optimized lattice parameters and space group symmetries as proposed by PLATON[24] are given in Table S5 along with the DFT optimized energy per unit cell, which is also compared in Figure S12. Interestingly, Li atoms on the site 2*b* in the space group $P6_3/mcm$, that is, the Li atoms in octahedral coordination, revealed a tendency to move from the center of the octahedron into the center of a shared triangular face (i.e., to the site 2*a*) during the optimizations of model 4. Starting and final positions of this Li atom as well as selected intermediate configurations are shown in Figure 2 together with the energy difference between octahedral and triangular coordinations of 1.8 eV/cell. These results motivated us to repeat the calculations of models 1, 3, 4, and 5 starting from a configuration that has Li occupying the center of the triangular face. Such a configuration turned out to be stable and had lower energy than the octahedral configurations for all recalculated models and approximations. Model 2 was not recalculated, because it is similar to model 1. The optimization of model 3, which was quite unstable, and the resulting energy always higher, in fact resulted in a crystal composed of positively (Mg-rich) and negatively (Li-rich) charged layers. Optimization of model 4 always produced a monoclinic distortion of the starting orthohexagonal cell, not observed by powder diffraction. The triangular coordination of Li is known from several oxides.[37] On the other hand, X-ray and neutron powder diffraction showed slight preference for the octahedral coordination of Li, that is, for the site 2*b*. We can conclude that models 1, 2, and 5 have similar and lowest energy, in agreement with the idea that a mixture of ordered domains with these models can produce a spatial average image of the hexagonal structure as observed by powder diffraction. It should however be kept in mind, that we do not have any information about an exact local arrangement of domains containing models 1, 2, and 5, that is, domain size and domain boundary. Additionally, the fact that these ordered models have the lowest DFT calculated energy does not necessarily guarantee that they exist in our samples prepared by our synthetic method. We can however conclude that Li is quite loosely localized within the $(BH_4)_6$ octahedron, and disordering of $Li_3MZn_5(BH_4)_{15}$ may lead to the Li conductivity along the octahedral channels. The CIF file of the DFT optimized model 1 (*Cmcm*) for $Li_3MgZn_5(BH_4)_{15}$ is given in the Supporting Information.

Interestingly, a similar octahedral coordination of Li within face-sharing octahedral chains was observed in a new ammine borohydride $LiMg(BH_4)_3(NH_3)_2$.[38] No deeper analysis of possible mobility of Li and its localization on the triangular face was performed in ref 38.

Ionic Conductivity. The sample b-Mg 10:2:4 reveals low ionic conductivity 4×10^{-8} S/cm at room temperature in agreement with lithium placed at the fully ordered octahedral site. The electronic conductivity is by 1 order lower, that is, of 4×10^{-9} S/cm as expected for partly covalently bonded framework structures. Preliminary measurement on manganese containing sample, b-Mn 13:2:5, provided similarly low ionic conductivity.

Structural Relations. The structure of hexagonal trimetallic $Li_3MZn_5(BH_4)_{15}$ is related to the orthorhombic bimetallic $LiZn_2(BH_4)_5$ (Figure 1) by the following:

$$a_{hex} \approx c_{ortho}, \quad c_{hex} \approx a_{ortho} \tag{6}$$

The pseudohegaxonal arrangement is visible in $LiZn_2(BH_4)_5$ in Figure 3, showing a structural fragment with an ideal hexagonal symmetry in $Li_3MZn_5(BH_4)_{15}$ and a pseudohexagonal

dx.doi.org/10.1021/ic401139k | *Inorg. Chem.* 2013, 52, 9941−9947

symmetry in $LiZn_2(BH_4)_5$, both drawn in bold. The relation between $Li_3MZn_5(BH_4)_{15}$ and $LiZn_2(BH_4)_5$ may also be understood as 1/6 of Zn^{2+} in $LiZn_2(BH_4)_5$ being replaced by Li^+ and the charge difference compensated by mixing the original Li site in $LiZn_2(BH_4)_5$ with M^{2+}, in agreement with the decomposition reaction of eq 3. Formation of the new compounds $Li_3MZn_5(BH_4)_{15}$ is facilitated by the chemical similarities mainly among Li/Mg/Zn and Mg/Mn, which allow cation disorder. Cation disorder is significantly less common than anion disorder, which occurs due to the similarities between BH_4 and the heavier halides.[39]

$Li_3MZn_5(BH_4)_{15}$ is the first trimetallic homoleptic borohydride ever observed, as the trimetallic $M_2Li[Y(BH_4)_{6-x}Cl_x]$ (M = Rb, Cs)[40] is mixed borohydride/chloride. $Li_3MZn_5(BH_4)_{15}$ contains two frameworks as observed for $LiZn_2(BH_4)_5$[8] (see Figures 1 and 3). While the loosely located Li either on the octahedral 2*b* or triangular 2*a* site allows for interpretation of the $Li_3MZn_5(BH_4)_{15}$ frameworks as interconnected or interpenetrated, respectively, the frameworks in $LiZn_2(BH_4)_5$ are interpenetrated. There are no $Zn_2(BH_4)_5$ dimers in the $Li_2MZn_5(BH_4)_{15}$ framework contrary to $LiZn_2(BH_4)_5$; however, the localization of Li on triangular 2*a* site leads to $LiZn(BH_4)_5$ dimers.

Topology Analysis. The frameworks of $Li_3MZn_5(BH_4)_{15}$ and $LiZn_2(BH_4)_5$ have been analyzed with the program TOPOS.[41] If the position of the loosely located Li atom in $Li_3MZn_5(BH_4)_{15}$ is fixed to the center of the triangular face (brings us back to sort of connected dimers, now Li−Zn dimers with a 90° twist of the triangular plane), it can be shown that while the underlying (3,4)-connected net in $LiZn_2(BH_4)_5$ is of **tfa**-c type (i.e., two interpenetrating **tfa** nets), the net in $Li_3MZn_5(BH_4)_{15}$ is of **mco**-c type (i.e., two interpenetrating **mco** nets with a basic tile built from three **tfa** tiles each), not yet observed among the known frameworks (see Figure S14). The framework of $Li_3MZn_5(BH_4)_{15}$ completes the known structural arrangements among the borohydrides exemplified by the tetrahedral framework in $Mg(BH_4)_2$[42,43] and $Mn(BH_4)_2$,[44] the octahedral framework in $Ca(BH_4)_2$[45] and $Y(BH_4)_3$,[46] the tetrahedral-octahedral framework in $KCd(BH_4)_3$[14] and $LiM(BH_4)_3Cl$, M = La, Gd, Ce,[47,48] and triangular-tetrahedral framework in $LiZn_2(BH_4)_5$.[8] The $Li_3MZn_5(BH_4)_{15}$ framework reveals that compact as well as porous frameworks containing differently coordinated cations in one framework can be built with the BH_4 ligand.

CONCLUSION

The compounds $Li_3MZn_5(BH_4)_{15}$, M = Mg or Mn, are the first trimetallic borohydrides, and constitute a new type of materials containing cationic solid solutions. The framework in $Li_3MZn_5(BH_4)_{15}$ has not previously been observed among known compounds. It contains channels built from face-sharing $(BH_4)_6$ octahedra. While X-ray and neutron powder diffraction shows a preference to locate lithium in the center of the octahedral site, thus resulting in two weakly interconnected frameworks of new type, the DFT calculations clearly favor lithium inside the shared triangular faces, leading to two interpenetrated **mco**-nets (**mco**-c type). Impedance spectroscopy has not shown significant lithium mobility in the crystal, but heterovalent substitution on Zn or mixed Mg/Li sites may be used to disorder the octahedral channels and thereby also to increase the lithium mobility and make these compounds attractive as solid-state electrolyte. As the compounds decompose to three known metal borohydrides, their application for hydrogen storage appears to be limited.

DFT calculations were used to model the local order on the disordered Mg/Li site. It was shown that locally the structure stabilizes upon maximizing Mg−Mg distances, thus leading to three different ordered models whose superposition simulates the hexagonal symmetry observed by the powder diffraction. However, no information about the coherent length of the orthorhombic structure is available either from our diffraction experiment or from our DFT modeling.

The presence of triangular $Zn(BH_4)_3$ and tetrahedral $Li/M(BH_4)_4$ building blocks in the same stable metal borohydride provides valuable knowledge for future crystal engineering of new open framework borohydrides.

ASSOCIATED CONTENT

Supporting Information

Rietveld refinement plots, T-ramps, DFT calculation results, and crystal data from refined and calculated models as CIF files. This material is available free of charge via the Internet at http://pubs.acs.org.

AUTHOR INFORMATION

Corresponding Author

*E-mail: radovan.cerny@unige.ch.

Notes

The authors declare no competing financial interest.

ACKNOWLEDGMENTS

This work was supported by the Swiss National Science Foundation, Slovak Grant Agency VEGA, under contract no. 2/0131/12, Ministry of Higher Education, Science and Technology of the Republic of Slovenia (MR-28339), Ad Futura Scholarship and CRUS Sciex Scholarship, and in part by the Danish National research Foundation (DNRF93), the Danish Strategic Research Council (HyFillFast). Part of the calculations were performed in the Computing Centre of the Slovak Academy of Sciences using the supercomputing infrastructure acquired in project ITMS 26230120002 and 26210120002 (Slovak Infrastructure for High-performance Computing) supported by the Research & Development Operational Programme funded by the ERDF. We are also grateful to SLS and ESRF for the provision of beam time, and to Yaroslav Filinchuk (SNBL) and to Denis Sheptyakov (PSI) for the help with powder diffraction data collection. We thank Raphael Janot (Université de Picardie - Jules Verne) for preliminary measurement of ionic conductivity of the manganese-containing sample.

REFERENCES

(1) Nakamori, Y.; Orimo, S. In *Solid-State Hydrogen Storage, Materials and Chemistry*; Walker, G., Ed.; Woodhead Publishing Ltd.: Cambridge, 2008; pp 420−449.

(2) Li, H.-W.; Yan, Y.; Orimo, S.; Züttel, A.; Jensen, C. M. *Energies* **2011**, *4*, 185−214.

(3) Ravnsbæk, D. B.; Filinchuk, Y.; Černý, R.; Jensen, T. R. *Z. Kristallogr.* **2010**, *225*, 557−569.

(4) Hagemann, H.; Longhini, M.; Kaminski, J. W.; Wesolowski, T. A.; Černý, R.; Penin, N.; Sorby, M. H.; Hauback, B. C.; Severa, G.; Jensen, C. M. *J. Phys. Chem. A* **2008**, *112*, 7551−7555.

(5) Černý, R.; Severa, G.; Ravnsbæk, D.; Filinchuk, Y.; D'Anna, V.; Hagemann, H.; Haase, D.; Jensen, C. M.; Jensen, T. R. *J. Phys. Chem. C* **2010**, *114*, 1357−1364.

(6) Černý, R.; Ravnsbæk, D.; Severa, G.; Filinchuk, Y.; D'Anna, V.; Hagemann, H.; Haase, D.; Skibsted, J.; Jensen, C. M.; Jensen, T. R. *J. Phys. Chem. C* **2010**, *114*, 19540−19549.
(7) Jaroń, T.; Grochala, W. *Dalton Trans.* **2011**, *40*, 12808−12817.
(8) Ravnsbæk, D.; Filinchuk, Y.; Cerenius, Y.; Jakobsen, H. J.; Besenbacher, F.; Skibsted, J.; Jensen, T. R. *Angew. Chem., Int. Ed.* **2009**, *48*, 6659−6663.
(9) Černý, R.; Ki Chul, K.; Penin, N.; D'Anna, V.; Hagemann, H.; Sholl, D. S. *J. Phys. Chem. C* **2010**, *114*, 19127−19133.
(10) Lindemann, I.; Domènech Ferrer, R.; Dunsch, L.; Filinchuk, Y.; Černý, R.; Hagemann, H.; D'Anna, V.; Lawson Daku, L. M.; Schultz, L.; Gutfleisch, O. *Chem.-Eur. J.* **2010**, *16*, 8707−8712.
(11) Lindemann, I.; Domènech Ferrer, R.; Dunsch, L.; Černý, R.; Hagemann, H.; D'Anna, V.; Filinchuk, Y.; Schultz, L.; Gutfleisch, O. *Faraday Discuss.* **2011**, *151*, 231−242.
(12) Černý, R.; Ravnsbæk, D. B.; Schouwink, P.; Filinchuk, Y.; Penin, N.; Teyssier, J.; Smrčok, L.; Jensen, T. R. *J. Phys. Chem. C* **2012**, *116*, 1563−1571.
(13) Schouwink, P.; D'Anna, V.; Brix Ley, M.; Lawson Daku, L. M.; Richter, B.; Jensen, T. R.; Hagemann, H.; Černý, R. *J. Phys. Chem. C* **2012**, *116*, 10829−10840.
(14) Ravnsbæk, D.; Sørensen, L. H.; Filinchuk, Y.; Besenbacher, F.; Jensen, T. R. *Angew. Chem., Int. Ed.* **2012**, *51*, 3582−3586.
(15) Černý, R.; Penin, N.; D'Anna, V.; Hagemann, H.; Durand, E.; Ruzicka, J. *Acta Mater.* **2011**, *59*, 5171−5180.
(16) Albanese, E.; Kalantzopoulos, G.; Vitillo, J. G.; Pinatel, E.; Civalleri, B.; Deledda, S.; Bordiga, S.; Hauback, B.; Baricco, M. *Book of Abstract, MH2012*, Kyoto, 2012; p 179.
(17) Kedrova, N. S.; Mal'tseva, N. N. *Russ. J. Inorg. Chem.* **1977**, *22*, 971−973;Translated from: *Zh. Neorg. Khim.* **1977**, *22*, 1791−1794.
(18) Hagemann, H.; Černý, R. *Dalton Trans.* **2010**, *39*, 60006−60012.
(19) Chłopek, K.; Frommen, Ch.; Léon, A.; Zabara, O.; Fichtner, M. *J. Mater. Chem.* **2007**, *17*, 3496−3503.
(20) Hammersley, A. P.; Svensson, S. O.; Hanfland, M.; Fitch, A. N.; Häusermann, D. *High Pressure Res.* **1996**, *14*, 235−248.
(21) Boultif, A.; Louer, D. *J. Appl. Crystallogr.* **2004**, *37*, 724−731.
(22) Favre-Nicolin, V.; Černý, R. *J. Appl. Crystallogr.* **2002**, *35*, 734−743.
(23) Coelho, A. A. TOPAS-Academic; http://members.optusnet.com.au/~alancoelho.
(24) Spek, A. L. *PLATON*; University of Utrecht: The Netherlands, 2006; Vol. 36. Kresse, G.; Hafner, J. *Phys. Rev. B* 1993, *48*, 13115−13118.
(25) Kresse, G.; Hafner, J. *Phys. Rev. B* **1993**, *48*, 13115−13118.
(26) (a) Kresse, G.; Furthmüller, J. *Phys. Rev. B* **1996**, *54*, 11169−11186. (b) Kresse, G.; Furthmüller, J. *Comput. Mater. Sci.* **1996**, *6*, 15−50.
(27) Paier, J.; Hirschl, R.; Marsman, M.; Kresse, G. *J. Chem. Phys.* **2005**, *122*, 234102.
(28) Mattsson, A. E.; Armiento, R.; Paier, J.; Kresse, G.; Wills, J. M.; Mattsson, T. R. *J. Chem. Phys.* **2008**, *128*, 084714.
(29) Grimme, S. *J. Comput. Chem.* **2006**, *27*, 1787−1799.
(30) Tkatchenko, A.; Scheffler, M. *Phys. Rev. Lett.* **2009**, *102*, 073005.
(31) Bučko, T.; Lèbegue, S.; Hafner, J.; Ángyán, G. *Phys. Rev.* **2013**, *87*, 064110.
(32) Blöchl, P. E. *Phys. Rev. B* **1994**, *50*, 17953−17979.
(33) Kresse, G.; Joubert, J. *Phys. Rev. B* **1999**, *59*, 1758−1775.
(34) Kresse, G.; Hafner, J. *J. Phys.: Condens. Matter* **1994**, *6*, 8245−8527.
(35) Ravnsbæk, D. B.; Frommen, C.; Reed, D.; Filinchuk, Y.; Sørby, M.; Hauback, B. C.; Jakobsen, H. J.; Book, D.; Besenbacher, F.; Skibsted, J.; Jensen, T. R. *J. Alloys Compd.* **2011**, *509S*, S698−S704.
(36) Filinchuk, Y.; Černý, R.; Hagemann, H. *Chem. Mater.* **2009**, *21*, 925−933.
(37) Sabrowsky, H.; Mertens, P.; Thimm, A. *Z. Kristallogr.* **1985**, *171*, 1−6.
(38) Sun, W.; Chen, X.; Gu, Q.; Wallwork, K. S.; Tan, Y.; Tang, Z.; Yu, X. *Chem.-Eur. J.* **2012**, *18*, 6825−6834.
(39) Rude, L. H.; Nielsen, T. K.; Ravnsbæk, D. B.; Bösenberg, U.; Ley, M. B.; Richter, B.; Arnbjerg, L. M.; Dornheim, M.; Filinchuk, Y.; Besenbacher, F.; Jensen, T. R. *Phys. Status Solidi A* **2011**, *208*, 1754−1773.
(40) Jaron, T.; Wegner, W.; Grochala, W. *Dalton Trans.* **2013**, accepted.
(41) Blatov, V. A. *Struct. Chem.* **2012**, *23*, 955−963.
(42) Černý, R.; Filinchuk, Y.; Hagemann, H.; Yvon, K. *Angew. Chem., Int. Ed.* **2007**, *46*, 5765−5767.
(43) Filinchuk, Y.; Richter, B.; Jensen, T. R.; Dmitriev, V.; Chernyshov, D.; Hagemann, H. *Angew. Chem., Int. Ed.* **2011**, *50*, 11162−11166.
(44) Černý, R.; Penin, N.; Hagemann, H.; Filinchuk, Y. *J. Phys. Chem. C* **2009**, *113*, 9003−9007.
(45) Filinchuk, Y.; Rönnebro, E.; Chandra, D. *Acta Mater.* **2009**, *57*, 732−738.
(46) Ravnsbæk, D. B.; Filinchuk, Y.; Černý, R.; Ley, M. B.; Haase, D.; Jakobsen, H. J.; Skibsted, J.; Jensen, T. R. *Inorg. Chem.* **2010**, *49*, 3801−3809.
(47) Ley, M. B.; Ravnsbæk, D. B.; Filinchuk, Y.; Lee, Y.-S.; Janot, R.; Cho, Y. W.; Skibsted, J.; Jensen, T. R. *Chem. Mater.* **2012**, *24*, 1654−1663.
(48) Ley, M. B.; Boulineau, S.; Janot, R.; Filinchuk, Y.; Jensen, T. R. *J. Phys. Chem. C* **2012**, *116*, 21267−21276.